

# MGVQ: Synergizing Multi-dimensional Sensitivity-Aware and Gradient-Hessian Fusion for Vector Quantization

Zhong Wang<sup>\*1</sup> Zukang Xu<sup>\*2</sup> Xing Hu<sup>2</sup> Dawei Yang<sup>2†</sup>

## Abstract

Vision-Language Models (VLMs) have demonstrated impressive capabilities. Nevertheless, their sheer scale presents a major obstacle to deployment on resource-constrained devices. Among compression strategies, vector quantization (VQ) emerges as a superior approach due to its high representational efficiency at ultra-low bitwidths. VQ operates by establishing a compact codebook where weight vectors are assigned to their nearest discrete codewords, thereby reducing memory footprint and bandwidth usage while maintaining the model’s performance. However, applying VQ directly to VLMs faces two fundamental challenges: (1) Modality-induced weight heterogeneity. In VLMs, image and text inputs induce divergent weight distributions, which a unified codebook fails to capture. (2) Error compensation mismatch from ignoring first-order gradients. In VLMs, existing second-order error compensation methods shift weights from pre-trained convergence points, ignoring gradient drift and leading to inaccurate loss with biased compensation. To overcome these hurdles, we introduce **MGVQ** (Synergizing **M**ulti-dimensional Sensitivity-Aware and **G**radient-Hessian Fusion for **V**ector **Q**uantization), a framework comprising two pivotal components: (1) Sensitivity-driven structured mixed-precision quantization, a mixed-precision scheme that allocates bit-widths based on channel sensitivity, combining global and local sensitivity metrics for fine-grained and interpretable resource distribution. (2) Gradient-aware second-order error compensation, a compensation method that explicitly incorporates first-order gradients to address their non-negligible role in VLM quantization errors, with efficient computation enabled by Kronecker and Block-

<sup>\*</sup>Equal contribution <sup>†</sup>Corresponding author. <sup>1</sup>Bauman Moscow State Technical University <sup>2</sup>Houmo AI. Correspondence to: Dawei Yang.

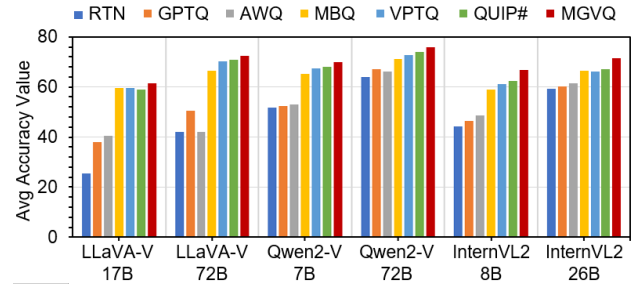


Figure 1. Comparison of average accuracy between MGVQ and other quantization methods across different VLMs

LDL decompositions. We validate MGVQ across leading VLMs, such as LLaVA-onevision, InternVL2, and Qwen2-VL. Under 2-bit quantization, our method consistently outperforms state-of-the-art PTQ baselines, delivering accuracy gains of up to **+4.9** (71.4% vs. 67.0% on InternVL2-26B). These results highlight MGVQ as a robust and efficient solution for ultra-low-bit quantization, facilitating the practical deployment of multimodal models in resource-constrained scenarios.

## 1. Introduction

Vision-Language Models (VLMs) are multimodal AI systems that integrate computer vision and natural language processing, taking both text and image/video inputs to generate text outputs, thereby enabling rich cross-modal reasoning and interaction (Bordes et al., 2024; Zhang et al., 2024a; Liu et al., 2023; Bai et al., 2023; Wang et al., 2024). However, these models typically contain billions of parameters, making training and inference computationally expensive and limiting their deployment in latency-sensitive or resource-constrained environments (Xue et al., 2025). For instance, Qwen2-VL-72B requires over 140GB of GPU memory during the prefill stage under FP16 inference, far exceeding the capacity of most edge devices. Reducing memory and bandwidth requirements while maintaining accuracy is therefore essential for practical deployment of large VLMs. Post-training quantization (PTQ) avoids expensive retraining and substantially reduces storage and

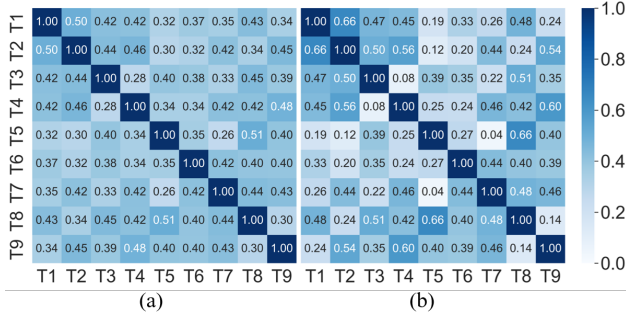


Figure 2. Similarity between tokens. (a) Text tokens similarity. (b) Image tokens similarity

memory bandwidth, making it a key technique for compressing LLMs (Frantar et al., 2022; Li et al., 2025b; Xu et al., 2025). Currently, PTQ methods can be broadly categorized into two classes. Scalar quantization (SQ), which performs well at medium to high bit-widths ( $\geq 4$  bits), assigns each weight an independent scaling factor and zero point, offering a lightweight representation (Frantar et al., 2022; Lin et al., 2023; Hu et al., 2024). Nevertheless, as the bitwidth decreases to 3 bits or lower, the representational capacity of SQ becomes severely limited, resulting in sharp accuracy degradation. In contrast, vector quantization (VQ) maps high-dimensional weight vectors into a shared codebook, exploiting structural redundancy to achieve higher compression ratios (Gersho, 1979). This approach has been shown to substantially improve quantization performance under ultra-low-bitwidth settings (Van Baalen et al., 2024; Liu et al., 2024b; Yue et al., 2025). However, directly applying vector quantization to VLMs leads to severe accuracy degradation due to two fundamental challenges: (1) Modality-induced weight heterogeneity. Within the same layer, VLM weights must simultaneously adapt to image and text tokens. As shown in Figure 2, these two types of tokens exhibit markedly different statistical characteristics, resulting in the heterogeneous weight distributions illustrated in Figure 3. Applying a unified codebook or fixed bit allocation across an entire layer fails to accommodate such structural heterogeneity, thereby amplifying quantization errors. (2) Error compensation mismatch from ignoring first-order gradients. Existing second-order error compensation methods inevitably shift weights away from their pre-trained convergence point. This displacement breaks the local optimality, inducing significant first-order gradients that were previously negligible, as illustrated in Figure 4. By relying solely on Hessian curvature, conventional methods such as YAQA (Tseng et al., 2025) and VPTQ (Liu et al., 2024b) neglect this gradient drift. Consequently, such an oversight causes inaccurate loss approximation and biased error compensation, ultimately degrading final model performance.

To address these limitations, we propose MGVQ (Syner-

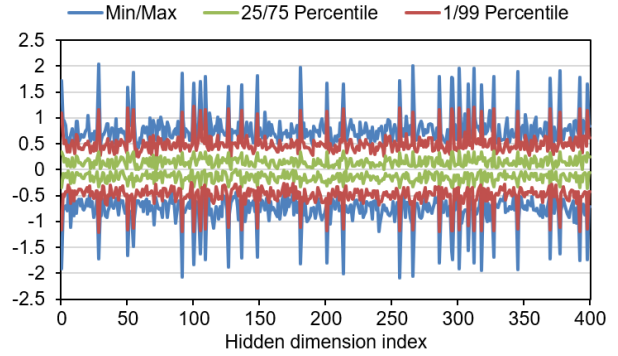


Figure 3. Weight distribution map of layer.1.down\_proj in LLaVA-OneVision-7B.

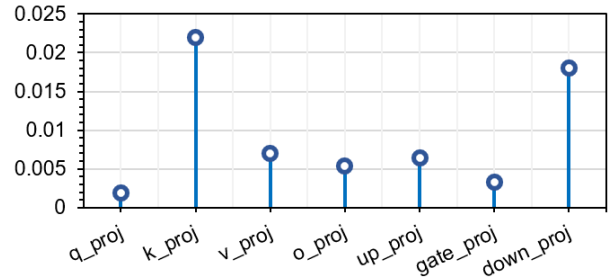


Figure 4. Gradient value at the 99% quantile of the gradient statistics of the 31st block of Qwen2-VL-72B after YAQA.

gizing Multi-dimensional Sensitivity-Aware and Gradient-Hessian Fusion for Vector Quantization), a quantization framework consisting of two key components: (1) Sensitivity-driven structured mixed-precision quantization (SSMQ). We integrate both global and local sensitivity metrics to partition sub-blocks of weights and allocate optimal bit under a fixed bit budget. Highly sensitive regions are assigned more bits, enabling fine-grained and interpretable resource allocation. (2) Gradient-aware error compensation (GAEC). For each layer, we perform a Taylor expansion of the global loss, where the quantization residual is used to approximate the first-order gradient matrix and the second-order Hessian is approximated via Kronecker factorization. Based on this formulation, we derive the theoretically optimal compensation rule and apply it iteratively to progressively reduce quantization errors.

These two components enable channel-level adaptive bit allocation and error compensation under resource-constrained conditions, while overcoming the limitation of conventional PTQ methods that neglect first-order gradient terms. This significantly alleviates the accumulation of quantization errors in deep networks and their adverse impact during cross-modal propagation. Experimental results show that under 2-bit quantization, as observed in Figure 1, MGVQ consistently outperforms existing approaches across multiple representative VLMs. For example, on the InternVL (Chen

et al., 2024b) model, MGVQ achieves more than a 4% improvement over QuIP# (Tseng et al., 2024), and ablation studies further validate the independent contributions of each module.

The main contributions of this paper are summarized as follows:

- We identify two VLM-specific challenges for vector quantization: modality-induced weight heterogeneity and error compensation mismatch from ignoring first-order gradients.
- We propose MGVQ, which combines multi-dimensional sensitivity analysis, structured mixed-precision allocation, and gradient-aware error compensation to mitigate cross-layer and cross-modal quantization errors.
- We conduct extensive experiments on representative VLMs, showing that MGVQ achieves superior accuracy under low bitwidth quantization while maintaining efficiency, outperforming existing state-of-the-art (SOTA) methods.

## 2. Related Work

**Scalar Quantization (SQ)** maps parameters to uniformly spaced levels using a shared scaling factor and zero-point, implicitly assuming isotropy in the parameter space and uniform channel sensitivity. Current SQ schemes, when combined with auxiliary optimization techniques, have demonstrated strong performance at 4-bit precision and above. Representative approaches include GPTQ (Frantar et al., 2022) and GuidedQuant (Kim et al., 2025), which leverage Hessian-based error compensation to mitigate quantization loss. QuaRot (Ashkboos et al., 2024) and OstQuant (Hu et al., 2025) leverage rotation matrices to transform the parameter space, thereby improving the distribution of weights and activations across the quantization domain. MQuant (Yu et al., 2025) and MBQ (Li et al., 2025a) enhance multimodal PTQ by addressing modality disparities and outliers through structured techniques and gradient-based balancing, respectively, yielding improved accuracy and efficiency. While these methods are hardware-friendly and straightforward to implement, the quantization error grows sharply below 4-bit, limiting practicality at ultra-low bit allocation.

In contrast to SQ, **Vector Quantization (VQ)** partitions weights into subvectors and approximates them using a codebook of limited prototypes. Compared with SQ, VQ offers stronger representational capacity and better accuracy retention under 3-bit and even lower precision. PCDVQ (Yue et al., 2025) decouples magnitude and direction in polar coordinates and uses distribution-aligned codebooks, delivering strong performance even at 2-bit precision. VPTQ (Liu

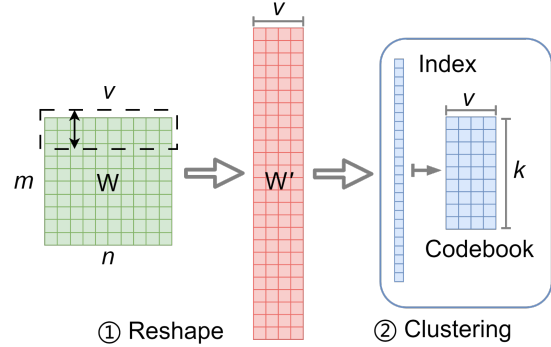


Figure 5. Vector Quantization.

et al., 2024b) employs channel-wise second-order optimization, efficient codebook initialization, and residual/outlier handling to achieve ultra-low-bit quantization, improving accuracy while reducing calibration time and boosting inference throughput. QuIP# (Tseng et al., 2024) achieves state-of-the-art extreme compression by integrating structured transforms, lattice codebooks, and lightweight fine-tuning, enabling 3-bit models to outperform 4-bit baselines.

A comprehensive investigation of vector quantization (VQ) for VLMs remains absent, and a general-purpose framework has yet to be established. Two fundamental challenges underpin this gap. First, modality-induced weight heterogeneity poses a significant hurdle, visual and textual tokens exhibit markedly different statistical properties, resulting in mixed-distribution weights that cannot be effectively represented by a unified codebook. Second, neglecting first-order gradients leads to error compensation mismatch, prevailing methods, such as GPTQ (Frantar et al., 2022) and YAQA (Tseng et al., 2025), operate under the assumption of near-zero gradients and consequently restrict compensation to second-order, Hessian-based approximations, thereby leaving first-order contributions unaccounted for. Some first-order enhanced methods, such as FOEM (Zheng et al., 2025), still retain a GPTQ-style row-wise formulation, modeling curvature per output channel rather than jointly across input and output channels at the layer level.

To tackle these gaps and challenges, we introduce MGVQ. The method integrates multi-dimensional sensitivity analysis, structured mixed-precision allocation, and gradient-aware compensation, and is specifically designed to optimize ultra-low-bit quantization for VLMs.

## 3. Preliminaries

**Vector Quantization in Post-Training Quantization.** In ultra-low-bit PTQ, VQ has attracted increasing attention due to its superior ability to model weight distributions and achieve higher compression ratios compared with scalar

quantization. The core idea of VQ is to jointly encode correlated dimensions within small subspaces, approximating each weight sub-vector with a finite set of codewords. Formally, consider a weight matrix  $W \in \mathbb{R}^{m \times n}$ . Given a block size  $v$  (with zero-padding applied if  $v \nmid mn$ ), the matrix is reshaped into:

$$W' \in \mathbb{R}^{M \times v}, \quad M = \frac{mn}{v}, \quad (1)$$

where the  $i$ -th row  $W'_i \in \mathbb{R}^{1 \times v}$  corresponds to a weight vector block of length  $v$ .

A codebook  $C \in \mathbb{R}^{K \times v}$  of size  $K = 2^n$  is then constructed, where  $n$  denotes the index bitwidth. Each vector block is quantized by selecting its nearest codeword from the codebook under Euclidean distance (noting that the Frobenius norm reduces to  $\ell_2$  distance in the vector case):

$$\text{VQ}(W') = \left\{ j_i \mid j_i = \arg \min_{j \in \{1, \dots, K\}} \|W'_i - C_j\|_2^2, \right. \\ \left. i = 1, \dots, M \right\}. \quad (2)$$

Finally, the quantized weight matrix  $\hat{W}$  is reconstructed by replacing each block with its assigned codeword and reshaping back to the original dimensions:

$$\hat{W} = \text{reshape}(\hat{W}', m, n). \quad (3)$$

This formulation highlights how VQ leverages clustering in a shared codebook to exploit structural redundancy, thereby retaining stronger representational capacity under ultra-low-bit settings compared to scalar quantization.

## 4. Method

The proposed MGVQ (Synergizing Multi-dimensional Sensitivity-Aware and Gradient-Hessian Fusion for Vector Quantization) framework is built on the coordinated design of two key modules: channel-sensitivity-driven structured mixed-precision quantization and gradient-aware error compensation. To address multimodal inputs (image tokens and text tokens), MGVQ first evaluates the sensitivity of input and output channels from both global sensitivity and local functional contribution, and fuses these metrics to form the basis for quantization resource allocation. The weight matrix is then reordered and partitioned into  $2 \times 2$  structured sub-blocks, followed by closed-form bit allocation under a global bit budget, ensuring that highly sensitive regions receive higher bitwidth. Finally, MGVQ incorporates both first-order gradient and second-order Hessian information to refine quantization results through fine-grained error compensation, achieving a balanced trade-off between model accuracy and compression efficiency. The detailed algorithmic procedures of the two modules are provided in Appendix A.5.

### 4.1. Sensitivity-driven structured mixed-precision quantization (SSMQ)

The primary focus in mixed-precision quantization lies in allocating limited bit budgets effectively, so that critical parameters receive finer precision. To this end, we design a channel-sensitivity-driven structured quantization framework, as observed in Figure 6, which proceeds in three steps: channel sensitivity assessment (CSA), matrix reordering and structured block partitioning (MRSBP), and optimal bit allocation (OBA).

#### Step 1: Channel Sensitivity Assessment (CSA)

When compressing models, it is essential to assess the global impact of perturbations. A straightforward approach is to directly measure changes in task-specific loss. Nevertheless, such an approach is often unreliable, as it depends heavily on the evaluation dataset and cannot be easily decomposed across layers. To establish a robust and decomposable metric, we construct channel sensitivity by integrating both global and local perspectives.

**Global sensitivity.** For a weight matrix  $W \in \mathbb{R}^{m \times n}$  (with  $m$  output channels and  $n$  input channels), we adopt the Hessian of the KL divergence (equivalent to the Fisher Information Matrix) as a measure of global sensitivity (see Appendix A.2 for the derivation). It is approximated by a Kronecker factorization:

$$H \approx H_O \otimes H_I, H_O \in \mathbb{R}^{m \times m}, H_I \in \mathbb{R}^{n \times n}, \quad (4)$$

where  $H_O$  denotes the output-side Hessian capturing sensitivity along output channels, and  $H_I$  denotes the input-side Hessian capturing sensitivity along input channels.

In practice, these components can be estimated from gradients at the sequence level:

$$H_I = \mathbb{E} [(\nabla_W \ell)^T (\nabla_W \ell)], \\ H_O = \mathbb{E} [(\nabla_W \ell) (\nabla_W \ell)^T], \quad (5)$$

where,  $\nabla_W \ell$  denotes the gradient of the loss  $\ell$  with respect to the weights  $W$ . The global sensitivity of input channel  $i$  is defined as the  $i$ -th diagonal element of  $H_I$ , and the global sensitivity of output channel  $j$  is defined as the  $j$ -th diagonal element of  $H_O$ . We denote these quantities as:

$$I_g^{(in)}[i] = H_I[i], I_g^{(out)}[j] = H_O[j]. \quad (6)$$

**Local Sensitivity.** To measure the extent of local output influence across weight channels in practical scenarios, we compute the corresponding norm value of output activations as local sensitivity. The local sensitivity of input-output reflects the output energy generated by activation  $x$  and

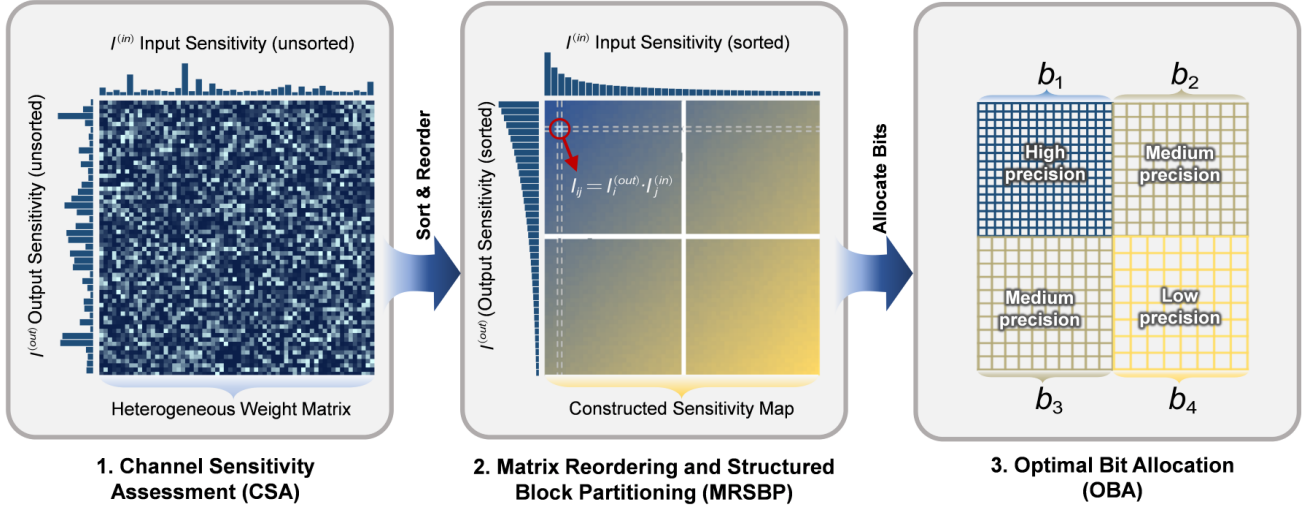


Figure 6. Overview of sensitivity-driven structured mixed-precision quantization (SSMQ)

weight  $W$  across corresponding channels:

$$\begin{aligned} I_l^{(in)}[i] &= \mathbb{E} [\|x \cdot W_{:,i}\|_2^2], \\ I_l^{(out)}[j] &= \mathbb{E} [\|x \cdot W_{j,:}\|_2^2]. \end{aligned} \quad (7)$$

**Combined Sensitivity.** The normalized global and local indicators are fused to obtain the final sensitivity scores:

$$\begin{aligned} I^{(in)}[i] &= \log\left(\hat{I}_g^{(in)}[i] \cdot \hat{I}_l^{(in)}[i]\right), \\ I^{(out)}[j] &= \log\left(\hat{I}_g^{(out)}[j] \cdot \hat{I}_l^{(out)}[j]\right), \end{aligned} \quad (8)$$

where  $\hat{\cdot}$  denotes min–max normalization. This fusion balances global and local sensitivity, enabling an accurate assessment of quantization difficulty. Consequently, it provides a reliable basis for bit allocation.

### Step 2: Matrix Reordering and Structured Block Partitioning (MRSBP)

To cluster parameters with similar sensitivity, we sort input and output channels in descending order of  $I^{(in)}$  and  $I^{(out)}$ . The reordered weight matrix  $W'$  is then partitioned into  $2 \times 2$  structured blocks. The sensitivity of each element  $(i, j)$  is defined as the product of the corresponding input and output channel sensitivity:

$$I_{i,j} = I^{(out)}[i] \cdot I^{(in)}[j]. \quad (9)$$

Given partitioning cut points along the input/output dimensions, the matrix is divided into four sub-blocks  $\{blk_t\}_{t=1}^4$ . With a total bit budget  $B$ , the goal is to allocate bits  $\{b_t\}$  to these sub-blocks to maximize the sensitivity–bit efficiency ratio:

$$\max_{\{b_t\}} \sum_{t=1}^4 \frac{S_t}{b_t}, \quad \text{s.t.} \quad \sum_{t=1}^4 b_t = B, \quad b_t > 0, \quad (10)$$

where  $S_t = \sum_{(i,j) \in blk_t} I_{i,j}$  is the aggregated sensitivity of block  $t$ . This ensures that more sensitive regions receive finer quantization.

### Step 3: Optimal Bit Allocation (OBA)

Applying Lagrangian optimization yields the closed-form solution for the optimal bit allocation:

$$b_t = \frac{B \cdot \sqrt{S_t}}{\sum_{s=1}^4 \sqrt{S_s}}. \quad (11)$$

This solution achieves the global optimum of Eq.10 in theory, ensuring the maximization of sensitivity return per bit of resource. The detailed derivation procedure is provided in Appendix A.1.

### 4.2. Gradient-Aware Error Compensation (GAEC)

To bridge the gap between quantization error minimization and task loss minimization, we introduce GAEC. It models the gradient drift caused by quantization (Zheng et al., 2025) and integrates it into a curvature-based compensation framework (Tseng et al., 2025), yielding compensation directions that better match the task loss.

#### Step 1: Formulating the Joint First- and Second-Order Optimization Objective

We frame the quantization problem as minimizing the task loss induced by the quantization residual. We define the residual  $E$  between the original floating-point weights  $W$  and their quantized counterparts  $\hat{W}$  as the core optimization variable:

$$E \triangleq W - \hat{W}. \quad (12)$$

Optimizing  $\hat{W}$  to minimize loss is mathematically equivalent to optimizing  $E$ . To render the high-dimensional

Hessian computationally tractable, we adopt a Kronecker-factored approximation ( $H \approx H_O \otimes H_I$ ). This structural simplification allows us to formulate the joint optimization objective as a quadratic form balancing first-order correction and second-order regularization:

$$\min_{\hat{W}} \underbrace{\text{vec}(E)^T \nabla \mathcal{L}}_{\text{First-order}} + \frac{1}{2} \underbrace{\text{vec}(E)^T (H_O \otimes H_I) \text{vec}(E)}_{\text{Second-order}}. \quad (13)$$

Here,  $H_O$  and  $H_I$  capture the output and input channel sensitivities, respectively. Conventional second-order methods typically assume a local optimum ( $\nabla \mathcal{L} \approx 0$ ), but accumulated quantization errors shift the weights away from the original optimum, inducing non-negligible first-order gradients. Neglecting this drift, or approximating it with an isotropic proxy ( $\nabla \mathcal{L} \approx \beta E$ ), yields compensation directions that are inconsistent with the curvature structure. To address this, at iteration  $t$ , we define the current residual as  $E^{(t)} = W - \hat{W}^{(t)}$  and explicitly approximate the gradient as the residual projected through the curvature:

$$\nabla \mathcal{L}^{(t)} \approx \beta (H_O \otimes H_I) \text{vec}(E^{(t)}), \quad \beta > 0, \quad (14)$$

where  $\beta$  controls the strength of the curvature-projected gradient correction. Substituting Eq.14 into the first-order term of Eq.13 yields the following convex quadratic subproblem in  $\text{vec}(E)$ :

$$\min_{\hat{W}} \beta \cdot \text{vec}(E)^T (H_O \otimes H_I) \text{vec}(E^{(t)}) + \frac{1}{2} \cdot \text{vec}(E)^T (H_O \otimes H_I) \text{vec}(E) \quad (15)$$

This formulation yields a curvature-aware and gradient-drift-aware compensation objective. It preserves the Kronecker structure for efficient block-wise solving while explicitly accounting for the non-negligible first-order effects induced by quantization.

## Step 2: Deriving the Curvature-Aligned Closed-Form Solution

To simplify optimization, we exploit the structure of the Hessian blocks via their block-LDL decompositions:

$$\begin{aligned} H_O &= (L_O + I) D_O (L_O + I)^T, \\ H_I &= (L_I + I) D_I (L_I + I)^T, \end{aligned} \quad (16)$$

where  $L_O, L_I$  are lower triangular matrices with zero diagonals,  $D_O, D_I$  are diagonal matrices of positive entries, and  $I$  is the identity matrix. We define  $Z$  and  $A^{(t)}$ :

$$\begin{aligned} Z &\triangleq (L_O + I)^T E (L_I + I), \\ A^{(t)} &\triangleq (L_O + I)^{-T} E^{(t)} (L_I + I)^{-1}. \end{aligned} \quad (17)$$

Then, Eq.15 can be decoupled element-wise into

$$\min_Z \sum_{i,j} \left[ \frac{1}{2} \lambda_{ij} Z_{ij}^2 + \beta \lambda_{ij} A_{ij}^{(t)} Z_{ij} \right], \quad (18)$$

where the curvature sensitivity is defined as:

$$\lambda_{ij} = D_O(i) D_I(j) > 0. \quad (19)$$

Differentiating Eq.18 with respect to  $Z_{ij}$ , the sensitivity term  $\lambda_{ij}$  acts on both the quadratic and linear terms and thus cancels out in the optimality condition. This yields a remarkably simple closed-form solution:

$$Z_{ij}^* = -\beta A_{ij}^{(t)}. \quad (20)$$

For the subsequent update step, we explicitly define the correction target  $T$  based on this optimal solution:

$$T \triangleq \beta A^{(t)}. \quad (21)$$

## Step 3: Fixed-Point Update Under Quantization Constraints (Projection)

We integrate second-order feedback and the above first-order correction into a single projection step. Let  $E^{(t)} = W - \hat{W}^{(t)}$ . Define the target

$$\eta \triangleq W + L_O^T E^{(t)} L_I + L_O^T E^{(t)} + E^{(t)} L_I - T, \quad (22)$$

and update by projection onto  $\mathcal{Q}$ :

$$\hat{W}^{(t+1)} \leftarrow \mathcal{Q}(\eta). \quad (23)$$

By iteratively solving Eq.23, GAEC efficiently finds the optimal quantized weights that balance both the immediate quantization error and the task-loss gradient drift. Notably, as  $\beta \rightarrow 0$ , the method reduces to the purely second-order update without the first-order correction.

## 5. Experiments

### 5.1. Experimental Settings

**Calibration set and evaluation benchmarks.** To collect the statistics required for quantization sensitivity analysis, we adopt the improved COCO image-caption dataset provided by ShareGPT4V (Chen et al., 2024a). A random subset of 128 image-text pairs is selected as the calibration set, which is used to compute Hessian information and channel importance scores. Model performance is evaluated with the LMMs-Eval benchmark suite (Zhang et al., 2024b) across a wide range of vision-language tasks, including: (1) Text recognition and understanding: OCRBench (Liu et al., 2024a) (scene text recognition), TextVQA (Singh et al., 2019) (text-centric visual question answering). (2) Visual perception: VizWiz (Gurari et al., 2018) (QA on everyday photos designed for visually impaired users), SEED-Bench (Li et al., 2024a) (a multimodal benchmark for generation and understanding). (3) Visual reasoning: ScienceQA (Lu et al., 2022) (science QA with multimodal inputs), MMMU (Yue et al., 2024) (multi-discipline multimodal understanding and reasoning).

Table 1. Under the 2-bit and 3-bit configurations of MGVQ, a comparison is conducted between it and diverse quantization methods of VLMs.

Bit	Method	LLaVA-onevision-7B	LLaVA-onevision-72B	Qwen2-VL-7B	Qwen2-VL-72B	InternVL2-8B	InternVL2-26B
3	FP16	66.9	74.3	73.1	78.1	71.7	74.6
	RTN	47.9	72.1	65.4	75.0	69.0	73.3
	GPTQ	63.4	72.3	67.9	76.6	67.2	72.3
	AWQ	60.4	55.1	70.3	77.5	69.8	73.5
	MBQ	64.8	73.6	70.9	77.6	70.4	73.8
	VPTQ	65.3	73.6	71.3	77.5	70.6	73.9
	MGVQ	65.8	74.0	71.9	77.8	71.1	74.2
2	RTN	25.5	42.2	51.8	64.0	44.3	59.4
	GPTQ	38	50.5	52.5	67.1	46.6	60.2
	AWQ	40.4	42.2	53.0	66.3	48.5	61.4
	MBQ	59.6	66.5	65.1	71.1	59.1	66.5
	VPTQ	59.6	70.2	67.3	72.6	61.3	66.3
	QuIP#	58.9	70.9	68.2	73.9	62.4	67.0
	MGVQ	61.5	72.4	70.0	75.8	66.7	71.4

Table 2. Ablation experiments on SSMQ and GAEC

Model	Bit	SSMQ	GAEC	MMM	SEED	OCRBench	VizWiz	ScienceQA	TextVQA	Average
LLaVA-onevision-7B	2	✗	✗	33.1	51.3	50.1	51.0	73.1	61.0	53.3
		✓	✗	38.9	65.1	52.3	55.8	82.1	67.9	60.4
		✗	✓	35.2	56.9	51.4	53.9	76.9	66.3	56.8
		✓	✓	40.1	66.3	54.5	56.1	83.1	68.9	61.5
Qwen2-VL-7B	3	✗	✗	41.4	63.2	68.3	61.4	81.1	71.4	64.5
		✓	✗	47.2	68.3	73.9	66.3	83.1	77.9	69.5
		✗	✓	45.9	68.9	69.6	65.6	82.2	76.9	68.2
		✓	✓	49.3	70.5	78.1	68.1	84.3	80.9	71.9

**Models and quantization settings.** We select three representative families of VLMs with both small and large versions to evaluate the generality of MGVQ: LLaVA-onevision (Li et al., 2024b)(parameter sizes of 7B and 72B, with the VLM backbone based on Qwen2-7B/72B and the vision encoder SigLIP-400M (Zhai et al., 2023)), InternVL2 (Chen et al., 2024b)(parameter sizes of 8B and 26B, with the VLM backbone InternLM2-8B/20B and the vision encoder InternViT-300M/6B). Qwen2-VL (Wang et al., 2024)(parameter sizes of 7B and 72B, with VLM backbone Qwen2-7B/72B and a vision encoder of 675M parameters). We evaluate 3-bit and 2-bit configurations for each model, comparing MGVQ against strong PTQ baselines. Scalar quantization (SQ) baselines include RTN (uniform quantization), GPTQ (Frantar et al., 2022)(Hessian-guided), AWQ (Lin et al., 2023) (outlier-aware), and MBQ (Li et al., 2025a) (recent mixed-precision method). Vector quantization (VQ) baselines include VPTQ (Liu et al., 2024b) and QuIP# (Tseng et al., 2024), the latter being state-of-the-art for LLMs.

**Implementation details.** MGVQ first performs row-column reordering of weight matrices, partitions them into four blocks, and applies vector quantization separately to each block. The vector length is set to 4. K-means clustering is initialized with k-means++ and run for 100 iterations. All experiments are conducted on NVIDIA RTX

A6000 GPUs.

5.2. Main Results

According to Table 1, we report the average accuracy across the six datasets introduced above. MGVQ consistently achieves the best overall accuracy under both 3-bit and 2-bit quantization settings. In 3-bit quantization, MGVQ outperforms the best existing baselines by 0.2–1.5 percentage points on average. For example, on Qwen2-VL-72B, MGVQ achieves 77.8%, slightly higher than MBQ (77.6%) and VPTQ (77.5%). In 2-bit quantization, the advantage of MGVQ is more pronounced, improving over the strongest baseline by 1.3–4.9 percentage points. On InternVL2-26B, MGVQ reaches 71.4%, compared to QuIP# (67.0%) and MBQ (66.5%). MGVQ also significantly narrows the gap between quantized and full-precision models. For instance, in the LLaVA-onevision-7B 2-bit case, the FP16 model achieves 66.9%, while MGVQ reaches 61.5% (only -5.4). By contrast, the best baseline (VPTQ/MBQ) scores 59.6% (-7.3). This demonstrates MGVQ’s effectiveness in mitigating quantization-induced accuracy loss. In addition, end-to-end inference efficiency results are reported in Appendix A.3, which show consistent speedups across both prefilling and decoding stages. Detailed per-dataset results for each model are provided in Appendix A.4.

### 5.3. Ablation Studies

We conduct ablations on LLaVA-onevision-7B (Li et al., 2024b) and Qwen2-VL-7B (Wang et al., 2024), focusing on 2-bit and 3-bit scenarios across text recognition, visual perception, and visual reasoning tasks. We study the necessity and contributions of two core modules: SSMQ (sensitivity-driven structured mixed-precision quantization), and GAEC (gradient-aware error compensation). Baselines include vanilla VQ (K-means), VPTQ, and GPTVQ.

**Joint effectiveness of SSMQ and GAEC.** As shown in Table 2, both modules are necessary and complementary. On LLaVA-onevision-7B (2-bit), without SSMQ/GAEC the average accuracy is only 53.3%. Adding SSMQ improves it to 60.4%, while GAEC alone yields 56.8%. Combining both achieves 61.5%, narrowing the FP16 gap to 5.4 and outperforming single-module gains by +1.2 and +4.7, respectively. On Qwen2-VL-7B (3-bit), the average score rises from 64.5% (no modules) to 71.9% (both modules), again showing strong synergy.

**Effectiveness of SSMQ.** Table 3 compares SSMQ with existing VQ methods. On LLaVA-onevision-7B (2-bit), vanilla VQ achieves 53.3%, VPTQ scores 59.6%, while SSMQ reaches 60.4%. Notably, in ScienceQA, accuracy improves from 73.1% (K-means) to 82.1%, and in TextVQA from 61.0% to 67.9%, validating SSMQ’s advantage in dynamically allocating precision to channels under hybrid-distribution weights in VLMs.

Table 3. Effectiveness of SSMQ on LLaVA-OneVision-7B under 2-bit quantization

Benchmark	Kmeans	VPTQ	OURS (SSMQ)
MMMU	33.1	38.7	38.9
SEED	51.3	64.6	65.1
OCRBench	50.1	51.1	52.3
VizWiz	51.0	55.3	55.8
ScienceQA	73.1	80.4	82.1
TextVQA	61.0	67.3	67.9
Average	53.3	59.6	60.4

**Effectiveness of GAEC.** From Table 4, GAEC improves over GPTVQ and VPTQ by explicitly incorporating first-order gradient terms into second-order error compensation. Traditional second-order approaches such as GPTVQ (65.7%) underestimate small gradient regions (0–0.001), leading to insufficient compensation. GAEC alleviates this by leveraging gradient residuals, achieving 68.2% on Qwen2-VL-7B (3-bit), surpassing GPTVQ (65.7%) and VPTQ (67.3%). Gains are especially evident on gradient-sensitive tasks: OCRBench improves from 67.1% to 69.6%, and MMMU from 43.9% to 45.9%, demonstrating reduced error accumulation across layers and modalities.

Table 4. Effectiveness of GAEC on Qwen2-VL-7B under 2-bit quantization.

Benchmark	GPTVQ	VPTQ	OURS (GAEC)
MMMU	43.9	44.9	45.9
SEED	65.2	68.1	68.9
OCRBench	67.1	67.2	69.6
VizWiz	63.2	65.6	65.6
ScienceQA	80.1	81.1	82.2
TextVQA	74.5	76.9	76.9
Average	65.7	67.3	68.2

## 6. Conclusion

This work addresses the unique challenges of applying vector quantization to vision-language models (VLMs), where modality-induced weight heterogeneity and the non-negligible role of first-order gradients lead to severe performance degradation under low-bit settings. We propose **MGVQ**, a multi-dimensional sensitivity-aware vector quantization framework that integrates (1) modality-induced weight heterogeneity, and (2) gradient-aware error compensation. By jointly leveraging global-local sensitivity measures and efficient Kronecker/Block-LDL decomposition, MGVQ achieves fine-grained bit allocation and accurate error correction. Extensive experiments across diverse VLM families (LLaVA-onevision, InternVL2, Qwen2-VL) and model scales (7B–72B) demonstrate that MGVQ consistently outperforms existing SQ and VQ baselines, especially in the extreme 2-bit regime. Notably, MGVQ significantly reduces the quantization–FP16 gap, highlighting its effectiveness in mitigating cross-modal error accumulation. Ablation studies further confirm the complementary contributions of sensitivity-driven allocation and gradient-aware compensation. Our findings suggest that well-founded quantization strategies are crucial for enabling efficient deployment of large-scale multimodal models. Beyond the immediate improvements in VLM quantization, the proposed MGVQ framework offers a general perspective on integrating structural sensitivity analysis and gradient-informed optimization, which may inspire future research on compressing and accelerating multimodal foundation models. In the future, we plan to extend MGVQ to more complex multimodal scenarios, such as video-language understanding and multi-task joint modeling, to further explore its generalization potential.

## 7. Impact Statement

This paper presents work whose goal is to advance the field of Machine Learning. There are many potential societal consequences of our work, none which we feel must be specifically highlighted here.

## References

- Ashkboos, S., Mohtashami, A., Croci, M. L., Li, B., Cameron, P., Jaggi, M., Alistarh, D., Hoefler, T., and Hensman, J. Quarot: Outlier-free 4-bit inference in rotated llms. *Advances in Neural Information Processing Systems*, 37:100213–100240, 2024.
- Bai, J., Bai, S., Yang, S., Wang, S., Tan, S., Wang, P., Lin, J., Zhou, C., and Zhou, J. Qwen-vl: A versatile vision-language model for understanding, localization, text reading, and beyond. *arXiv preprint arXiv:2308.12966*, 2023.
- Bordes, F., Pang, R. Y., Ajay, A., Li, A. C., Bardes, A., Petryk, S., Mañas, O., Lin, Z., Mahmoud, A., Jayaraman, B., et al. An introduction to vision-language modeling. *arXiv preprint arXiv:2405.17247*, 2024.
- Chen, L., Li, J., Dong, X., Zhang, P., He, C., Wang, J., Zhao, F., and Lin, D. Sharegpt4v: Improving large multi-modal models with better captions. In *European Conference on Computer Vision*, pp. 370–387. Springer, 2024a.
- Chen, Z., Wu, J., Wang, W., Su, W., Chen, G., Xing, S., Zhong, M., Zhang, Q., Zhu, X., Lu, L., et al. Internvl: Scaling up vision foundation models and aligning for generic visual-linguistic tasks. In *Proceedings of the IEEE/CVF conference on computer vision and pattern recognition*, pp. 24185–24198, 2024b.
- Frantar, E., Ashkboos, S., Hoefler, T., and Alistarh, D. Gptq: Accurate post-training quantization for generative pre-trained transformers. *arXiv preprint arXiv:2210.17323*, 2022.
- Gersho, A. Asymptotically optimal block quantization. *IEEE Transactions on information theory*, 25(4):373–380, 1979.
- Gurari, D., Li, Q., Stangl, A. J., Guo, A., Lin, C., Grauman, K., Luo, J., and Bigham, J. P. Vizwiz grand challenge: Answering visual questions from blind people. In *Proceedings of the IEEE conference on computer vision and pattern recognition*, pp. 3608–3617, 2018.
- Hu, X., Cheng, Y., Yang, D., Yuan, Z., Yu, J., Xu, C., and Zhou, S. I-llm: Efficient integer-only inference for fully-quantized low-bit large language models. *arXiv preprint arXiv:2405.17849*, 2024.
- Hu, X., Cheng, Y., Yang, D., Xu, Z., Yuan, Z., Yu, J., Xu, C., Jiang, Z., and Zhou, S. Ostquant: Refining large language model quantization with orthogonal and scaling transformations for better distribution fitting. *arXiv preprint arXiv:2501.13987*, 2025.
- Kim, J., Halabi, M. E., Park, W., Schaefer, C. J., Lee, D., Park, Y., Lee, J. W., and Song, H. O. Guidedquant: Large language model quantization via exploiting end loss guidance. *arXiv preprint arXiv:2505.07004*, 2025.
- Li, B., Ge, Y., Ge, Y., Wang, G., Wang, R., Zhang, R., and Shan, Y. Seed-bench: Benchmarking multimodal large language models. In *Proceedings of the IEEE/CVF Conference on Computer Vision and Pattern Recognition*, pp. 13299–13308, 2024a.
- Li, B., Zhang, Y., Guo, D., Zhang, R., Li, F., Zhang, H., Zhang, K., Zhang, P., Li, Y., Liu, Z., et al. Llava-onevision: Easy visual task transfer. *arXiv preprint arXiv:2408.03326*, 2024b.
- Li, S., Hu, Y., Ning, X., Liu, X., Hong, K., Jia, X., Li, X., Yan, Y., Ran, P., Dai, G., et al. Mbq: Modality-balanced quantization for large vision-language models. In *Proceedings of the Computer Vision and Pattern Recognition Conference*, pp. 4167–4177, 2025a.
- Li, Y., Yin, R., Lee, D., Xiao, S., and Panda, P. Gptaq: Efficient finetuning-free quantization for asymmetric calibration. *arXiv preprint arXiv:2504.02692*, 2025b.
- Lin, J., Tang, J., Tang, H., Yang, S., Chen, W.-M., Wang, W.-C., Xiao, G., Dang, X., Gan, C., and Han, S. Awq: Activation-aware weight quantization for llm compression and acceleration. *arXiv preprint arXiv:2306.00978*, 2023.
- Liu, H., Li, C., Wu, Q., and Lee, Y. J. Visual instruction tuning. *Advances in neural information processing systems*, 36:34892–34916, 2023.
- Liu, Y., Li, Z., Huang, M., Yang, B., Yu, W., Li, C., Yin, X.-C., Liu, C.-L., Jin, L., and Bai, X. Ocrbench: on the hidden mystery of ocr in large multimodal models. *Science China Information Sciences*, 67(12):220102, 2024a.
- Liu, Y., Wen, J., Wang, Y., Ye, S., Zhang, L. L., Cao, T., Li, C., and Yang, M. Vptq: Extreme low-bit vector post-training quantization for large language models. *arXiv preprint arXiv:2409.17066*, 2024b.
- Lu, P., Mishra, S., Xia, T., Qiu, L., Chang, K.-W., Zhu, S.-C., Tafjord, O., Clark, P., and Kalyan, A. Learn to explain: Multimodal reasoning via thought chains for science question answering. *Advances in Neural Information Processing Systems*, 35:2507–2521, 2022.

- Singh, A., Natarajan, V., Shah, M., Jiang, Y., Chen, X., Batra, D., Parikh, D., and Rohrbach, M. Towards vqa models that can read. In *Proceedings of the IEEE/CVF conference on computer vision and pattern recognition*, pp. 8317–8326, 2019.
- Tseng, A., Chee, J., Sun, Q., Kuleshov, V., and De Sa, C. Quip#: Even better llm quantization with hadamard incoherence and lattice codebooks. *arXiv preprint arXiv:2402.04396*, 2024.
- Tseng, A., Sun, Z., and De Sa, C. Model-preserving adaptive rounding. *arXiv preprint arXiv:2505.22988*, 2025.
- Van Baalen, M., Kuzmin, A., Koryakovskiy, I., Nagel, M., Couperus, P., Bastoul, C., Mahurin, E., Blankevoort, T., and Whatmough, P. Gptvq: The blessing of dimensionality for llm quantization. *arXiv preprint arXiv:2402.15319*, 2024.
- Wang, P., Bai, S., Tan, S., Wang, S., Fan, Z., Bai, J., Chen, K., Liu, X., Wang, J., Ge, W., et al. Qwen2-vl: Enhancing vision-language model’s perception of the world at any resolution. *arXiv preprint arXiv:2409.12191*, 2024.
- Xu, Z., Yue, Y., Hu, X., Yuan, Z., Jiang, Z., Chen, Z., Yu, J., Xu, C., Zhou, S., and Yang, D. Mambaquant: Quantizing the mamba family with variance aligned rotation methods. *arXiv preprint arXiv:2501.13484*, 2025.
- Xue, Y., Huang, Y., Shao, J., and Zhang, J. Vlmq: Efficient post-training quantization for large vision-language models via hessian augmentation. *arXiv preprint arXiv:2508.03351*, 2025.
- Yu, J., Zhou, S., Yang, D., Li, S., Wang, S., Hu, X., Xu, C., Xu, Z., Shu, C., and Yuan, Z. Mquant: Unleashing the inference potential of multimodal large language models via static quantization. In *Proceedings of the 33rd ACM International Conference on Multimedia*, pp. 1783–1792, 2025.
- Yue, X., Ni, Y., Zhang, K., Zheng, T., Liu, R., Zhang, G., Stevens, S., Jiang, D., Ren, W., Sun, Y., et al. Mmmu: A massive multi-discipline multimodal understanding and reasoning benchmark for expert agi. In *Proceedings of the IEEE/CVF Conference on Computer Vision and Pattern Recognition*, pp. 9556–9567, 2024.
- Yue, Y., Xu, Z., Yuan, Z., Yang, D., Wu, J., and Nie, L. Pcdvq: Enhancing vector quantization for large language models via polar coordinate decoupling. *arXiv preprint arXiv:2506.05432*, 2025.
- Zhai, X., Mustafa, B., Kolesnikov, A., and Beyer, L. Sigmoid loss for language image pre-training. In *Proceedings of the IEEE/CVF international conference on computer vision*, pp. 11975–11986, 2023.
- Zhang, J., Huang, J., Jin, S., and Lu, S. Vision-language models for vision tasks: A survey. *IEEE transactions on pattern analysis and machine intelligence*, 46(8):5625–5644, 2024a.
- Zhang, K., Li, B., Zhang, P., Pu, F., Cahyono, J. A., Hu, K., Liu, S., Zhang, Y., Yang, J., Li, C., et al. Lmms-eval: Reality check on the evaluation of large multimodal models. *arXiv preprint arXiv:2407.12772*, 2024b.
- Zheng, X., Qin, H., Li, Y., Chu, H., Wang, J., Guo, J., Magno, M., and Liu, X. First-order error matters: Accurate compensation for quantized large language models. *arXiv preprint arXiv:2507.11017*, 2025.

## A. Appendix

### A.1. Closed-form Solution for Optimal Bit Allocation

The optimal bit allocation  $\{b_t\}_{t=1}^4$  that minimizes the objective

$$\min_{\{b_t\}} \sum_{t=1}^4 \frac{S_t}{b_t}, \quad \text{s.t.} \quad \sum_{t=1}^4 b_t = B, \quad b_t > 0, \quad (24)$$

where  $S_t = \sum_{(i,j) \in \text{blk}_t} I_{i,j}$  is the total sensitivity of block  $t$ , is given by the closed-form expression:

$$b_t = \frac{B \cdot \sqrt{S_t}}{\sum_{s=1}^4 \sqrt{S_s}}, \quad t = 1, \dots, 4. \quad (25)$$

*Proof.* Define the Lagrangian:

$$\mathcal{L}(b_1, \dots, b_4, \lambda) = \sum_{t=1}^4 \frac{S_t}{b_t} + \lambda \left( B - \sum_{t=1}^4 b_t \right). \quad (26)$$

Taking the derivative with respect to  $b_t$  and setting it to zero gives:

$$\frac{\partial \mathcal{L}}{\partial b_t} = -\frac{S_t}{b_t^2} - \lambda = 0 \quad \Rightarrow \quad \frac{S_t}{b_t^2} = -\lambda. \quad (27)$$

Hence,

$$\frac{S_1}{b_1^2} = \dots = \frac{S_4}{b_4^2} = c, \quad (28)$$

for some constant  $c$ , leading to

$$b_t = \sqrt{\frac{S_t}{c}}. \quad (29)$$

Applying the constraint  $\sum_{t=1}^4 b_t = B$ , we obtain

$$c = \left( \frac{\sum_{t=1}^4 \sqrt{S_t}}{B} \right)^2. \quad (30)$$

Substituting  $c$  yields the closed-form solution

$$b_t = \frac{B \cdot \sqrt{S_t}}{\sum_{s=1}^4 \sqrt{S_s}}. \quad (31)$$

This ensures that more bits are allocated to blocks with larger sensitivity, achieving globally optimal efficiency.

### A.2. Global Sensitivity via KL Divergence

In model compression, directly evaluating task loss changes is often unreliable, as it depends on specific datasets and cannot be decomposed across layers. Instead, we adopt the Kullback–Leibler (KL) divergence between the outputs of the full-precision model and the quantized model as a principled measure of quantization sensitivity.

Given a full-precision model  $M(W, X)$  with parameters  $W$  and its quantized counterpart  $M(\hat{W}, X)$ , the global KL loss is defined as:

$$\mathcal{L}_{\text{KL}}(\hat{W}) = \mathbb{E}_{X \sim \mathcal{D}} D_{\text{KL}}(M(W, X) \| M(\hat{W}, X)) \quad (32)$$

where  $X \sim \mathcal{D}$  denotes inputs drawn from the data distribution  $D$ . For small perturbations around  $W$ , a second-order Taylor expansion yields:

$$\mathcal{L}_{\text{KL}}(\hat{W}) \approx \frac{1}{2} (\hat{W} - W)^T H_{\text{global}} (\hat{W} - W) \quad (33)$$

where  $H_{global}$  is the Hessian of the KL divergence, equivalent to the Fisher Information Matrix:

$$H_{global} = \mathbb{E} \left[ \nabla_W \ell \nabla_W \ell^T \right] \quad (34)$$

Thus, the global Hessian provides a second-order sensitivity metric for weight perturbations, forming the theoretical basis for sensitivity analysis and bit allocation in our quantization framework.

### A.3. Additional Results

Table 5. The end-to-end speed up of LLaVA-onevision-7B on RTX4090 with fused GPU kernels. Experimental results show that our method achieves approximately 9% (W3) and 15% (W2) acceleration over FP16 on the Vision Transformer (ViT), delivers an average improvement of about 7–13% in the VLM Prefill stage, and reaches up to 37% acceleration in the Decoder stage, demonstrating the inference efficiency of our approach.

Model	Stage (tokens)	FP16 (ms)	W3 (ms)	W2 (ms)
ViT	Prefill (729)	11.5	10.5	9.7
VLM	Prefill (512)	68.1	61.3	59.8
	Prefill (1024)	108.6	100.5	94.7
	Decode	29.3	18.4	25.6

### A.4. All Results

Table 6. Results of LLaVA-onevision-7B.

Bit	Method	MMMU	SEED	OCRBench	VizWiz	ScienceQA	TextVQA	Average (↑)
FP16	-	46.0	71.1	62.2	60.4	85.4	76.1	66.9
3	RTN	34.7	10.4	35.9	59.2	86.2	60.9	47.9
	GPTQ	41.9	68.7	55.7	56.4	86.4	71.3	63.4
	AWQ	36.6	51.5	59.3	58.5	83.2	73.0	60.4
	MBQ	42.0	66.4	61.1	60.7	85.0	73.3	64.8
	VPTQ	43.3	69.1	61.4	60.2	84.7	73.1	65.3
	MGVQ	44.0	69.9	61.5	60.3	85.1	73.9	65.8
2	RTN	13.9	0.0	10.3	36.8	61.3	30.4	25.5
	GPTQ	30.2	8.5	29.7	50.1	70.3	39.4	38.0
	AWQ	30.9	9.8	35.3	50.3	71.9	43.9	40.4
	MBQ	37.6	63.5	52.0	56.1	81.2	67.5	59.6
	VPTQ	38.7	64.6	51.1	55.3	80.4	67.3	59.6
	QuIP#	37.7	62.3	51.0	55.2	80.3	67.1	58.9
	MGVQ	40.1	66.3	54.5	56.1	83.1	68.9	61.5

Table 7. Results of LLaVA-onevision-72B.

Bit	Method	MMMU	SEED	OCRBench	VizWiz	ScienceQA	TextVQA	Average (↑)
FP16	-	56.1	78.1	73.2	69.2	90.0	79.3	74.3
3	RTN	53.9	77.4	68.2	66.1	89.5	77.4	72.1
	GPTQ	52.7	76.0	69.7	68.3	89.3	77.9	72.3
	AWQ	33.4	71.2	48.7	49.3	69.2	58.8	55.1
	MBQ	54.4	77.6	71.6	69.0	90.3	78.5	73.6
	VPTQ	54.5	77.8	71.9	69.1	90.0	78.4	73.6
	MGVQ	55.6	77.9	72.5	69.0	90.1	79.0	74.0
2	RTN	34.5	18.5	34.5	50.1	71.1	44.4	42.2
	GPTQ	47.2	30.1	40.3	58.4	74.0	52.9	50.5
	AWQ	33.0	17.9	31.2	54.9	69.2	47.1	42.2
	MBQ	48.1	70.4	67.1	60.2	83.8	69.1	66.5
	VPTQ	51.3	74.6	69.0	66.3	86.8	72.9	70.2
	QuIP#	52.5	75.3	69.9	66.5	86.8	74.6	70.9
	MGVQ	53.4	75.8	71.7	68.1	87.9	77.4	72.4

Table 8. Results of InternVL2-8B.

Bit	Method	MMMU	SEED	OCRBench	VizWiz	ScienceQA	TextVQA	Average (↑)
FP16	-	48.0	71.6	76.5	61.1	96.2	77.0	71.7
3	RTN	43.7	70.3	74.0	56.0	95.6	74.6	69.0
	GPTQ	41.7	68.9	70.2	59.9	89.5	73.1	67.2
	AWQ	44.8	70.4	74.7	58.9	95.5	74.2	69.8
	MBQ	46.9	70.8	75.1	58.7	95.6	75.1	70.4
	VPTQ	47.1	70.9	75.4	59.1	95.5	75.8	70.6
	MGVQ	47.6	71.3	75.9	59.5	95.6	76.5	71.1
2	RTN	33.5	10.2	34.1	50.9	72.2	65.1	44.3
	GPTQ	30.4	18.9	37.9	48.1	77.9	66.3	46.6
	AWQ	34.5	20.7	38.2	53.2	75.8	68.8	48.5
	MBQ	40.3	65.8	50.4	53.3	77.3	67.3	59.1
	VPTQ	44.9	64.9	57.3	55.2	77.1	68.1	61.3
	QuIP#	45.3	67.3	61.2	54.1	78.2	68.4	62.4
	MGVQ	46.2	69.3	68.4	57.6	86.4	72.3	66.7

Table 9. Results of InternVL2-26B.

Bit	Method	MMMU	SEED	OCRBench	VizWiz	ScienceQA	TextVQA	Average ( $\uparrow$ )
FP16	-	47.1	76.8	77.9	66.2	97.5	82.1	74.6
3	RTN	46.6	75.7	75.9	64.7	96.4	80.6	73.3
	GPTQ	44.8	75.8	76.0	60.9	96.3	80.1	72.3
	AWQ	46.4	76.2	76.4	64.5	96.7	81.0	73.5
	MBQ	47.1	76.3	76.5	64.5	97.3	81.1	73.8
	VPTQ	47.3	76.0	76.9	65.2	97.1	81.0	73.9
	MGVQ	47.1	76.4	77.3	65.0	97.3	81.8	74.2
2	RTN	36.2	55.6	63.5	56.1	73.4	71.4	59.4
	GPTQ	37.4	58.2	64.3	55.1	72.4	73.8	60.2
	AWQ	38.4	55.4	64.9	57.4	74.9	77.4	61.4
	MBQ	43.2	65.3	70.2	58.4	83.9	78.1	66.5
	VPTQ	42.4	67.4	72.3	55.1	80.3	80.1	66.3
	QuIP#	44.2	69.3	71.2	56.1	80.3	81.1	67.0
	MGVQ	46.1	73.9	73.2	60.3	93.6	81.1	71.4

Table 10. Results of Qwen2-VL-7B.

Bit	Method	MMMU	SEED	OCRBench	VizWiz	ScienceQA	TextVQA	Average ( $\uparrow$ )
FP16	-	50.6	71.9	80.7	68.3	85.1	82.0	73.1
3	RTN	44.9	69.8	60.0	65.2	81.5	71.2	65.4
	GPTQ	43.1	68.9	74.8	64.3	79.7	76.7	67.9
	AWQ	44.7	70.4	76.9	68.0	82.5	79.5	70.3
	MBQ	47.9	70.2	76.8	67.7	82.8	79.9	70.9
	VPTQ	48.3	70.5	77.6	67.9	83.4	79.9	71.3
	MGVQ	49.3	70.5	78.1	68.1	84.3	80.9	71.9
2	RTN	36.5	55.9	50.4	45.9	71.8	50.3	51.8
	GPTQ	37.3	57.2	50.7	44.8	70.9	54.3	52.5
	AWQ	38.7	58.1	51.0	44.3	70.8	55.2	53.0
	MBQ	43.9	67.3	59.8	66.4	81.2	72.2	65.1
	VPTQ	44.9	68.1	67.2	65.6	81.1	76.9	67.3
	QuIP#	45.6	69.0	66.9	66.4	83.1	78.4	68.2
	MGVQ	46.8	68.9	74.9	67.1	83.4	79.0	70.0

Table 11. Results of Qwen2-VL-72B.

Bit	Method	MMMU	SEED	OCRBench	VizWiz	ScienceQA	TextVQA	Average ( $\uparrow$ )
FP16	-	61.1	77.6	79.9	76.0	91.6	82.5	78.1
3	RTN	57.7	77.5	70.4	74.8	89.7	79.7	75.0
	GPTQ	57.3	77.2	78.5	73.6	91.5	81.6	76.6
	AWQ	59.6	77.6	79.6	75.4	90.4	82.4	77.5
	MBQ	59.6	77.7	79.4	75.6	90.5	82.5	77.6
	VPTQ	59.4	77.6	79.0	75.8	90.9	82.1	77.5
	MGVQ	60.6	77.7	79.3	75.8	91.4	82.2	77.8
2	RTN	42.1	66.9	61.3	62.3	80.2	71.3	64.0
	GPTQ	44.2	68.1	66.3	65.4	82.5	75.8	67.1
	AWQ	44.5	67.3	66.9	64.3	80.4	74.5	66.3
	MBQ	48.9	71.4	74.9	69.8	82.9	78.4	71.1
	VPTQ	53.2	73.4	76.4	69.1	83.4	79.8	72.6
	QuIP#	55.8	73.9	76.1	72.3	85.8	79.5	73.9
	MGVQ	58.8	75.9	78.0	73.1	87.9	81.3	75.8

### A.5. Algorithm

---

**Algorithm 1** SSMQ: Sensitivity-driven Structured Mixed-precision Quantization

---

**Require:** Weight matrix  $W \in \mathbb{R}^{m \times n}$ , total bit budget  $B$

**Ensure:** Quantized weights  $\hat{W}$

- 1: **CSA: Channel Sensitivity Assessment**
  - 2: Compute Hessian factors  $H_I, H_O$  via Kronecker approximation (Eq. 5)
  - 3: **for** each input/output channel **do**
  - 4:   Compute global sensitivity (diag of  $H_I, H_O$ ) and local sensitivity (activation norm) (Eq. 6, 7)
  - 5:   Fuse normalized scores:  $I^{(in/out)} = \log(\hat{I}_g^{(in/out)} \cdot \hat{I}_l^{(in/out)})$  (Eq. 8)
  - 6: **end for**
  - 7: **MRSBP: Reordering & Partitioning**
  - 8: Sort channels by  $I^{(in)}$  and  $I^{(out)}$ , define sensitivity  $I_{i,j} = I^{(out)}[i] \cdot I^{(in)}[j]$  (Eq. 9)
  - 9: Partition  $W$  into four blocks and compute block sensitivity  $S_t$  (Eq. 10)
  - 10: **OBA: Optimal Bit Allocation**
  - 11: **for** each block  $t$  **do**
  - 12:    $b_t = B \cdot \frac{\sqrt{S_t}}{\sum_{s=1}^4 \sqrt{S_s}}$ , then quantize block with  $b_t$  bits
  - 13: (Eq. 11)
  - 14: **end for**
  - 15: **return**  $\hat{W}$
-

---

**Algorithm 2** GAEC: Gradient-Aware Error Compensation

---

**Require:** Original weights  $W$ , Hessian blocks  $H_O, H_I$ , quantizer  $\mathcal{Q}$ , scaling factor  $\beta$ , tolerance  $\varepsilon$ , maximum iterations  $K$

**Ensure:** Optimized quantized weights  $\hat{W}$

- 1: **Initialization**
  - 2:  $(L_O, D_O) = \text{BlockLDL}(H_O)$
  - 3:  $(L_I, D_I) = \text{BlockLDL}(H_I)$
  - 4:  $\hat{W} = \mathcal{Q}(W); t = 0$
  - 5: **Iterative Compensation**
  - 6: **while**  $t < K$  and not converged **do**
  - 7:    $E^{(t)} = W - \hat{W}^{(t)}$
  - 8:    $A^{(t)} = (L_O + I)^{-T} E^{(t)} (L_I + I)^{-1}$  (Eq. 17)
  - 9:    $T = \beta A^{(t)}$ . (Eq. 21)
  - 10:    $\eta = W + L_O^T E^{(t)} L_I + L_O^T E^{(t)} + E^{(t)} L_I - T$  (Eq. 22)
  - 11:    $\hat{W}_{\text{new}} = \mathcal{Q}(\eta)$  (Eq. 23)
  - 12:    $\Delta = \frac{\|\hat{W}_{\text{new}} - \hat{W}\|_F}{\max(1, \|\hat{W}\|_F)}$
  - 13:   **if**  $\Delta < \varepsilon$  **then**
  - 14:     break
  - 15:   **end if**
  - 16:    $\hat{W} = \hat{W}_{\text{new}}; t = t + 1$
  - 17: **end while**
  - 18: **return**  $\hat{W}$
-